Computer Methods in Biomechanics and Biomedical Engineering

Publication details, including instructions for authors and subscription information:
http://www.tandfonline.com/loi/gcmb20

Towards automatic measurement of anteversion and neck-shaft angles in human femurs using CT images

Casciaro E. Mariano [a] & Damian Craiem [a b]

[a] Electronics Department, FICEN, Favaloro University, Av. Belgrano 1723, CP 1093, Ciudad de Buenos Aires, Argentina

[b] CONICET, Buenos Aires, Argentina

Available online: 30 Mar 2012

To cite this article: Casciaro E. Mariano & Damian Craiem (2012): Towards automatic measurement of anteversion and neck-shaft angles in human femurs using CT images, Computer Methods in Biomechanics and Biomedical Engineering, DOI:10.1080/10255842.2012.672561

To link to this article: http://dx.doi.org/10.1080/10255842.2012.672561

Computer Methods in Biomechanics and Biomedical Engineering
iFirst article, 2012, 1–9

Towards automatic measurement of anteversion and neck–shaft angles in human femurs using CT images

Casciaro E. Mariano[a] and Damian Craiem[a,b]*

[a]*Electronics Department, FICEN, Favaloro University, Av. Belgrano 1723, CP 1093, Ciudad de Buenos Aires, Argentina;* [b]*CONICET, Buenos Aires, Argentina*

(*Received 7 June 2011; final version received 29 February 2012*)

Automatic assessment of human femur morphology may provide useful clinical information with regard to hip and knee surgery, prosthesis design and management of hip instability. To this end, neck–shaft and anteversion angles are usually used. We propose a full automatic method to estimate these angles in human femurs. Multislice CT images from 18 dried bones were analysed. The algorithm fits 3D cylinders to different regions of the bone to estimate the angles. A manual segmentation and a conventional angle assessment were used for validation. We found anteversion angle as $20 \pm 7°$ and neck–shaft angle as $130 \pm 9°$. Mean distances from femur surface to cylinders were 5.5 ± 0.6, 3.5 ± 0.6 and 2.4 ± 0.4 mm for condyles, diaphysis and neck regions, respectively. Automatic and conventional angles were positively correlated ($r^2 > 0.85$). Manual and automatic segmentations did not differ. The method was fast and 100% reproducible. A robust *in vivo* segmentation algorithm should be integrated to advance towards a clinically compliant methodology.

Keywords: human femora; anteversion; multislice computed tomography; 3D cylinder

1. Introduction

The assessment of human femur morphology provides useful information for assisted hip and knee surgery, prosthesis design and fracture management (Schmutz et al. 2006; Gargouri and de Guise 2007; Citak et al. 2009; Pearle et al. 2009). Computed tomography (CT) techniques allow accurate 3D bone reconstruction (Subburaj et al. 2009). As part of morphometric information related to human femora, some angles raised particular attention, such as femoral neck anteversion, which is involved in hip stability and hip range of motion following total hip arthroplasty (Lee et al. 1992; Isaac et al. 1997; Tayton 2007; Toogood et al. 2009; Birkenmaier et al. 2010). Conventional methods to estimate femoral angles are based on planar projections, although some 3D computer models were also reported (Sugano et al. 1998; Kim et al. 2000a; Gargouri and de Guise 2007; Citak et al. 2009). Methods based on 2D projections have limited reproducibility due to user manual intervention (Sugano et al. 1998; Kim et al. 2000b). Three dimentional approaches require complex reconstruction routines that limit their clinical applicability. From this perspective, given a 3D representation of the bone, an ideal system should accurately estimate femoral angles, without operator supervision, and avoiding numerically intensive algorithms.

Two angles of the human femur are particularly important: anteversion and neck–shaft angles. They are defined using neck, long and condylar axes (Isaac et al. 1997; Kim et al. 2000a). Each axis corresponds to specific regions of the femur that should be separated by anatomical landmarks. Details of proximal and distal femur anatomy must be carefully examined to properly isolate these regions (Schmutz et al. 2006; Toogood et al. 2009).

Recently, we have reported a cylinder fitting method to estimate coronary bifurcation angles (Craiem et al. 2009) and then we modified it to estimate femoral angles in a preliminary study (Casciaro et al. 2010). Even if the fitted surfaces were not strictly cylindrical, the advantage of this approach was that two cylinders unambiguously define a single angle in a 3D hyperspace. However, we found that the cylinder fitting method required some modifications for certain regions of the femur and that user intervention should be minimised.

In this study, we present a fully automatic method to estimate anteversion and neck–shaft angles in dried human femurs without user intervention. Right and left femurs from 10 donors were scanned using multislice CT. The methodology was implemented in a software program that processed the images in two steps. First, an automatic subdivision algorithm localises and isolates the diaphysis, condyles and neck regions. Second, three virtual cylinders are fitted to each region and their centreline vectors are used to automatically estimate the angles. The subdivision algorithm was validated against an expert manual separation. The automatic angle assessment was compared with a conventional 2D method (Hoiseth et al. 1989). For each bone region, the cylindrical fit accuracy was also quantified.

*Corresponding author. Email: dcraiem@favaloro.edu.ar

ISSN 1025-5842 print/ISSN 1476-8259 online

http://dx.doi.org/10.1080/10255842.2012.672561
http://www.tandfonline.com

2. Materials and methods

The methodology is organised as follows: Section 2.1 explains the image acquisition method, then Sections 2.2 and 2.3 includes the automatic region subdivision of the bone and finally Sections 2.4 and 2.5.explain the angle estimation. A validation procedure is proposed in Sections 2.6 and 2.7. The whole set of algorithms was carried out using MATLAB® in a standard 2.66 GHz PC.

2.1 Femoral bone surface acquisition

A total of 20 paired, fresh-frozen femora (10 right and 10 left) were selected from the bone bank of the Hospital Italiano (Buenos Aires, Argentina) for this Institutional Review Board-approved study from patients (60% male gender) aged 35.9 ± 12.0 y.o. (range of 16–58 y.o.). All the bones were scanned on a Toshiba Aquilion CT scanner, with a resolution of 0.877 pixels/mm and slice increments of 0.5 mm. The scanner in the Hospital follows a regular calibration twice every year. To avoid inter-scan variability and bias in surface acquisition for this study, all dried bones were piled and scanned together in a single sequence (Kim et al. 2000a). Afterwards, each bone was manually isolated using a custom software. The bones were not scanned in any particular position, and bone surface was obtained from the raw grey scale images by applying a Laplacian filter and subsequent binarisation (values > 100 Houndsfield units; Gonzalez and Woods 1992; Craiem et al. 2009). The spatial (x, y, z) coordinates of each pixel belonging to the femur surface were stored in a file. As shown in Figure 1(a), we defined the entire group of points representing the femoral surface as F, the surface of diaphyseal region as D, condylar region as C, proximal epiphyseal region as E, femoral neck as N and the femoral head as H.

2.2 Condylar, diaphysis and epiphysis subdivision

The process to separate C, D and E regions from F is based on a 'folding transformation' of the bone around its centreline and a partition of the enveloping curve in three sections. First, a Hotteling Transform (Gonzalez and Woods 1992) is carried out on the whole femoral surface F to estimate the main axial direction of the femur as shown in Figure 1(b). With this transform, the orientation of the bone was automatically assessed. Then, a cylinder is adjusted to the femoral surface F. The cylinder is fitted minimising the orthogonal distances from each point of F to a theoretical cylinder surface by means of Nelder–Mead simplex algorithm (implemented in the *fminsearch* Matlab function; Craiem et al. 2009). The algorithm requires three initial conditions: the direction vector, the radius and an arbitrary point. Accordingly, the main axis from the Hotteling transform, mean distance of each point to this line and the centre of mass are, respectively, used. At the end, the cylinder is completely defined by a direction vector and a rough radius as shown in Figure 1(c).

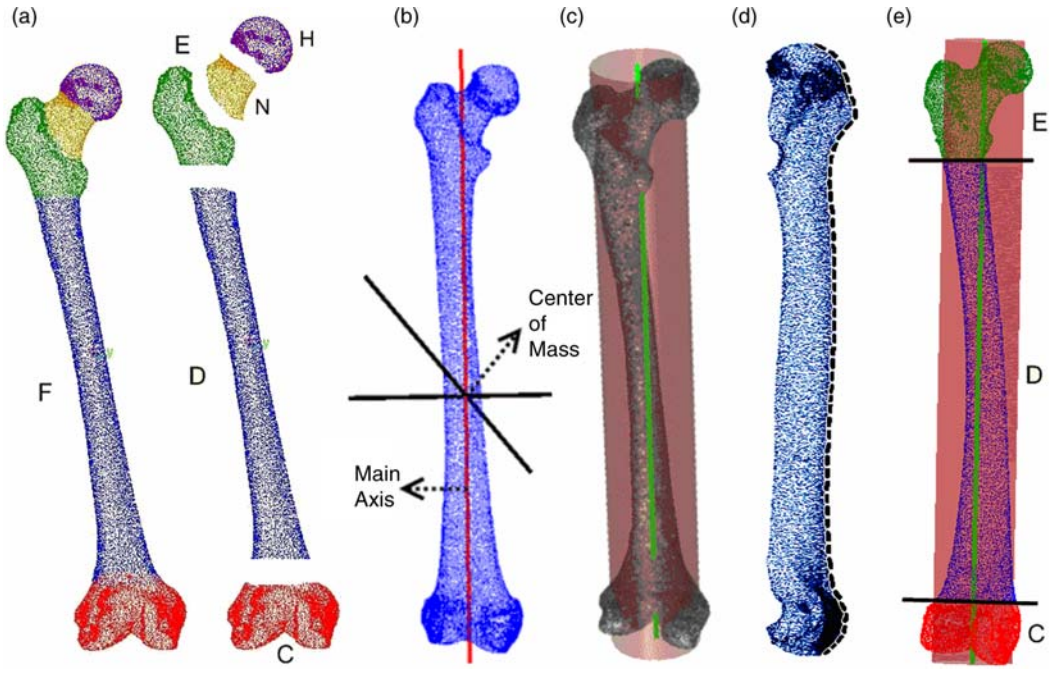

Figure 1. (a) Femoral surface points *F*, separated into diaphysis *D*, condyles *C* and proximal epiphysis *E*. Region E includes the femoral neck *N* and femoral head *H*. (b) Hotteling transform of *F* showing the main axial direction and centre of mass. (c) Cylindrical fit of *F*. (d) Folding transformation of F with a dashed line representing the enveloping curve. (e) Preliminary segmentation of C, D and E regions.

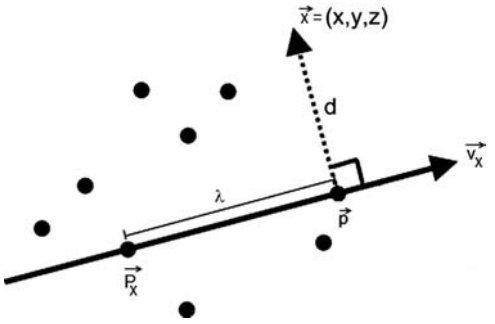

Figure 2. Projection $\vec{p}$ of a scatter point $\vec{x} = (x, y, z)$ onto a line $L = \lambda \vec{\nu}_X + \vec{P}_X$, where $\vec{\nu}_X$ is the normalised direction vector, d is the orthogonal distance between $\vec{p}$ and $\vec{x}$ and λ is the distance between an arbitrary point $\vec{P}_X$ and $\vec{p}$.

Once a raw cylinder is obtained, all surface points F are projected to a 2D transformed plane as shown in Figure 1(d). This operation is geometrically equivalent to carrying out a 'folding' of the femur around the cylinder centreline and will be referred as a 'folding transformation'. Basically, coordinates are transformed from (x, y, z) euclidean position in space to (λ, d) coordinates, where d is the orthogonal distance from each point to the cylinder centreline and λ is the longitudinal distance to the projection of an arbitrary point $\vec{P}_X$ lying on this centreline (Figure 2). The projection of the centre of mass of F onto the cylinder axis line was adopted as the $\vec{P}_X$ reference point.

For the folded femur, the enveloping curve is calculated as shown with a dashed line in Figure 1(d). The first derivative of the enveloping curve is used to determine two transition points to separate the femoral diaphysis (D) from condylar (C) and proximal epiphyseal (E) regions. To separate the femur in these three regions, two threshold levels were fixed with respect to maximum derivative values of the enveloping curve (Figure 3). Accordingly, a threshold level of 50% was chosen to separate region D from region C and a level of 25% to separate D from E. Percentages were empirically chosen taking into account the transition smoothness between the different regions. The (λ, d) space is finally divided into three regions: C, E and D. Lastly, as shown in Figure 1(e), all the points are re-projected to the (x, y, z) euclidean space, resulting in a preliminary isolation of condylar, diaphyseal and proximal epiphyseal regions.

2.3 *Segmentation of femoral neck and head*

Instead of using a 'folding transformation', the neck and head are separated in the epiphyseal region using an 'unfolding transformation'. First, the E region is fitted with a cylinder as shown in Figure 4(a). Then, the epiphyseal region is unfolded around the cylinder centreline but holding the unfolding angle α as an additional parameter. Accordingly, each (x, y, z) surface point in E is transformed into a (λ, d, α) coordinate system, where α is the unfolding angle. A vector $\vec{\nu}_{\text{ref}}$ orthogonal to cylinder centreline and connecting the most proximal point of the E is considered the $\alpha = 0$ reference angle. We call this transformation an 'unfolding transformation' because the resulting projection is equivalent to unfolding the E region surface around its centreline as shown in Figure 4(b). Using the Matlab

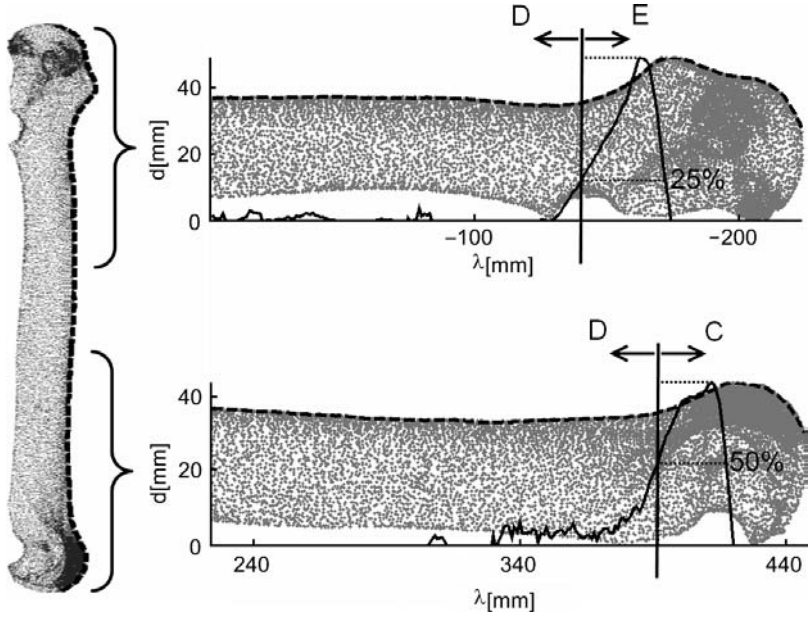

Figure 3. Proximal and distal femur portions. Dashed line represents the enveloping curve and solid line shows its derivative. Dotted lines indicate maximum derivatives and threshold levels of 25% and 50% to separate diaphyseal (D) from epiphyseal (E) and condylar (C) regions, respectively.

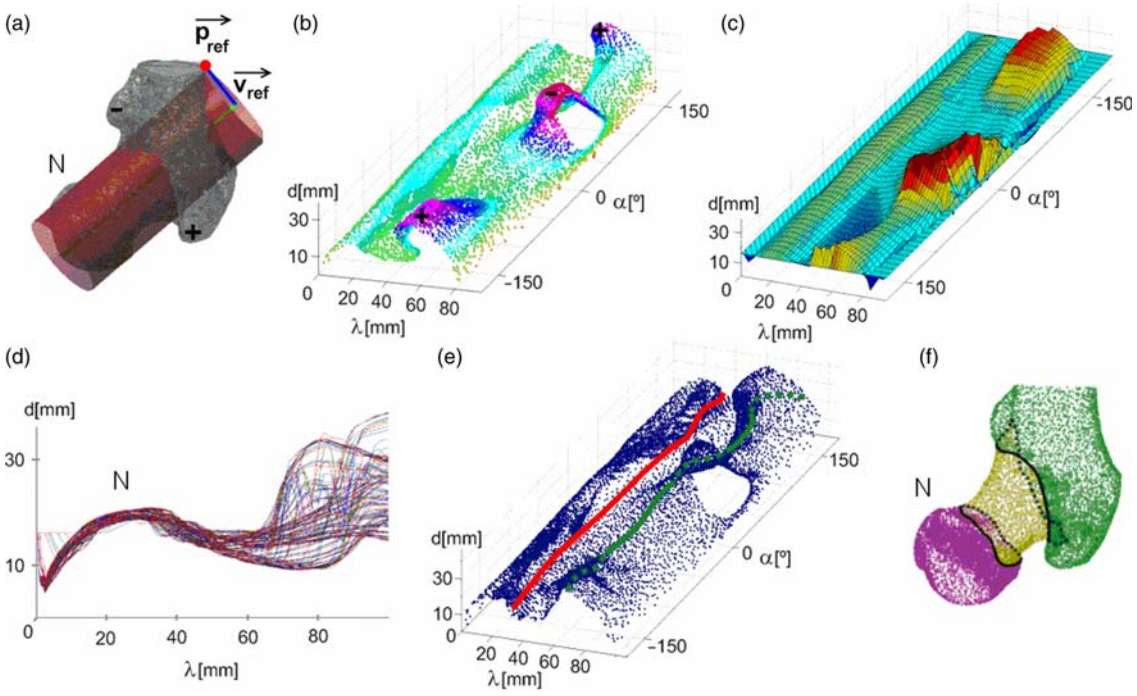

Figure 4. (a) Cylinder fitting of the epiphyseal region E. The most proximal point $\vec{p}_{\text{ref}}$ and a normal vector to cylinder centreline $\vec{\nu}_{\text{ref}}$ are used as unfolding angle $\alpha = 0°$ reference. (b) Unfolding transformation of E where colours are proportional to distance from cylinder centreline. (c) Interpolated surface. (d) The curves corresponding to the intersection between the surface and planes with constant unfolding angle α. (e) Unfolded E region. In green, the divisory line between N and trochanteral region. In red, divisory line between N and H. (f) Re-projected E region to euclidean coordinates. Within the figure, N = femoral neck and positive/negative signs = greater and lesser trochanter, respectively.

functions *griddata* and *spaps*, the points (λ, d, α) are grouped in a 1 mm by 1° grid and interpolated to a smooth surface as shown in Figure 4(c).

To separate the neck and the head, the intersection between this surface and planes with constant unfolding angle α is calculated and plotted into curves as shown in Figure 4(d). For each curve, the first-order derivative is calculated. Starting from mean λ, the first maximum derivatives values are calculated to the left and to the right. Maximum derivative points are adopted as the transitions between neck and trochanteric lines and between neck and femoral head. The sequential concatenation of maximum derivative points for every unfolding angle α is shown in Figure 4(e), creating two curves that separate the head and the neck from the rest of the epiphysis. Both curves are smoothed with a five-element moving average filter. Points are re-projected from (λ, d, α) to the (x, y, z) original coordinate system.

A final correction is applied to the neck region. An additional cylindrical fitting is carried out to the union of neck and head points obtained in the previous separation. Then, every point with a distance greater than 25% of the cylinder radius, and not belonging to H, is discarded from the neck. Accordingly, most of the spurious points belonging to the greater trochanter which have erroneously stayed in the neck region are now assigned to the correct group. The final head and neck segmentation is shown in Figure 4(f).

2.4 *Condylar, diaphysis and neck axis estimation*

In this section, condylar, diaphysis and neck axis will be estimated from isolated regions C, D and N, respectively, fitting cylinders to each region. Femoral anteversion and neck–shaft angles will be calculated from these axes. A preliminary result of the three fitted cylinders is shown in Figure 8(a). Some modifications were introduced into the fitting algorithm to take into account the particular geometrical features in each region. Details are given in the following paragraphs.

- *Diaphysis cylinder fitting:* Region D is directly adjusted with the original cylinder fitting algorithm (Craiem et al. 2009). The cylinder centreline will be adopted as the long axis of the femur.
- *Neck cylinder fitting:* The femoral neck has a cylindrical shape but in some cases it is too short, causing the fitting algorithm to misinterpret the centreline direction. Therefore, the algorithm was modified so as to fit a cylinder that minimises the orthogonal distances to the neck surface but is forced to pass through the centre of mass of the

femoral head (points H). This constraint fixes a point where the cylinder vector must pass and ensures a proper centreline determination for the neck in cases when it is too short.

- *Condylar cylinder fitting*: The cylinder fitting algorithm was conceived to adjust cylinders without caps. However, the condylar points C represent a closed surface, where left and right condyles have a different size. If the original algorithm is applied, condyles axes would show a misalignment with respect to the ground line (Figure 6, left), without conforming to the anteversion definition. To solve this particular problem, a modified version of the algorithm was implemented. In the original version, orthogonal distances to the femur surface are minimised (Craiem et al. 2009). We modified the minimisation function f for each iteration i, weighting the distances with a coefficient Δ_i

$$f = \sqrt{\sum_{i=1}^{N} \Delta_i (R - d_i)^2},$$

where d_i is the orthogonal distance of a point to the cylinder centreline, R is cylinder radius and Δ_i is the weighting function shown in Figure 5. Accordingly, every point that lies inside the cylinder ($d < R$) has less weight in the minimisation algorithm, whereas points outside the cylinder ($d > R$) are not affected ($\Delta = 1$). As shown in Figure 6 (right), a better parallelism between the cylinder axis and the ground line connecting the condyles is obtained.

2.5 Angle calculation

Using the three axes obtained in the previous section, two angles were automatically calculated. The following definitions are used:

- $\boldsymbol{\nu}_c$: centreline vector of the condylar cylinder (condylar axis);
- $\boldsymbol{\nu}_d$: centreline vector of the diaphysis cylinder (long axis);
- $\boldsymbol{\nu}_e$: centreline vector of the femoral neck (neck axis);
- $\boldsymbol{\nu}_N = \boldsymbol{\nu}_c \times \boldsymbol{\nu}_d$: vector normal to $\boldsymbol{\nu}_c$ and $\boldsymbol{\nu}_d$;
- $\boldsymbol{\nu}_P = \boldsymbol{\nu}_d \times \boldsymbol{\nu}_N$: projection vector normal to $\boldsymbol{\nu}_d$ and $\boldsymbol{\nu}_N$;
- $\Pi_{c/d} = \alpha\boldsymbol{\nu}_C + \beta\boldsymbol{\nu}_D$: plane formed by $\boldsymbol{\nu}_c$ and $\boldsymbol{\nu}_d$;
- $\Pi_P = \alpha\boldsymbol{\nu}_P + \beta\boldsymbol{\nu}_N$: $\boldsymbol{\nu}_c$ and $\boldsymbol{\nu}_e$ projection plane.

The angle between a pair of vectors $\vec{\boldsymbol{\nu}}_1$ and $\vec{\boldsymbol{\nu}}_2$ is calculated as

$$\cos(\theta) = \frac{\vec{\boldsymbol{\nu}}_1 \cdot \vec{\boldsymbol{\nu}}_2}{\|\vec{\boldsymbol{\nu}}_1\| . \|\vec{\boldsymbol{\nu}}_2\|}.$$

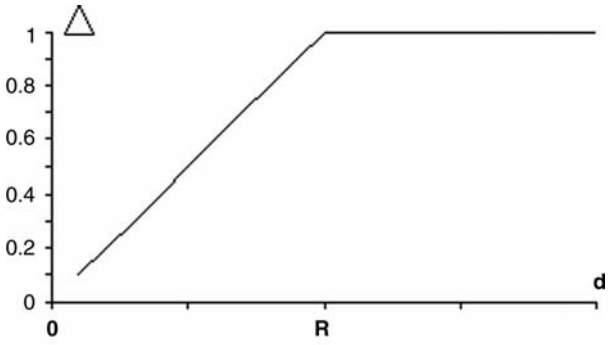

Figure 5. Weighting function Δ included into the modified cylinder fitting algorithm to reduce the influence of the caps of the condylar region. Points inside the cylinder of radius R, with distances to centreline $d < R$ are penalised, having less impact in the cylinder determination.

Accordingly, neck–shaft angle is calculated between vectors ($\boldsymbol{\nu}_e, \boldsymbol{\nu}_d$) (Figure 8). Anteversion is defined as the angle between the vector resulting from the projection of $\boldsymbol{\nu}_e$ and $\boldsymbol{\nu}_c$ over Π_P (Sugano et al. 1998). In other words, this is equivalent to an observer standing over the plane crossing the femur through its condylar and diaphyseal regions, $\Pi_{c/d}$, observing perpendicular to Π_P, measuring the angle between the floor and the resultant projection of the femoral neck on his plane of view (Figures 7 and 8).

2.6 Validation of the automatic region subdivision

To validate the automatic region subdivision, a custom brush tool was included in the developed program, allowing an expert orthopaedic surgeon to manually paint with different colours the five regions from Figure 1(a). Then, the corresponding cylinder fitting algorithms were applied to regions C, D and N and femoral angles were compared with respect to the automatic method values.

2.7 Validation of the automatic angle assessment

To validate the angle assessment, we compared the automatic results with a conventional 2D method of Reikeras in which the neck axis is determined from a superimposed image of the femoral head and neck (Hoiseth et al. 1989). Neck–shaft angle was manually measured with virtual calipers by the same expert using planar projections (Isaac et al. 1997; Toogood et al. 2009). A planar projection tool was also included in the developed software.

Differences between automatic and conventional methods were evaluated with Pearson correlations and residues were analysed in Bland–Altman plots. Values were also compared with paired t-test using $p < 0.05$ as significant level.

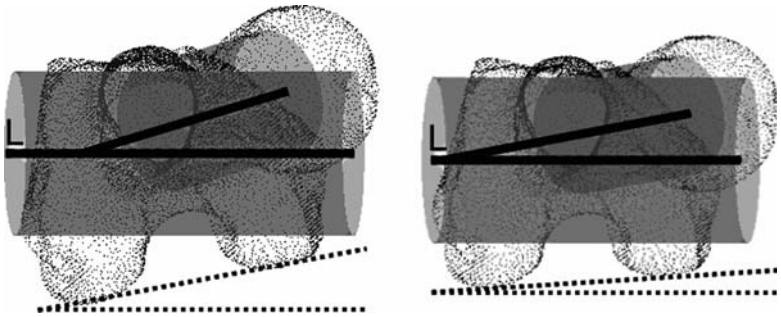

Figure 6. Cylinder fitting of the condyles region with the original minimisation algorithm (left) and after a modification to reduce the influence of the epicondyles (right). The result is an improved parallelism between the cylinder centreline and the ground line connecting the condyles (dotted lines).

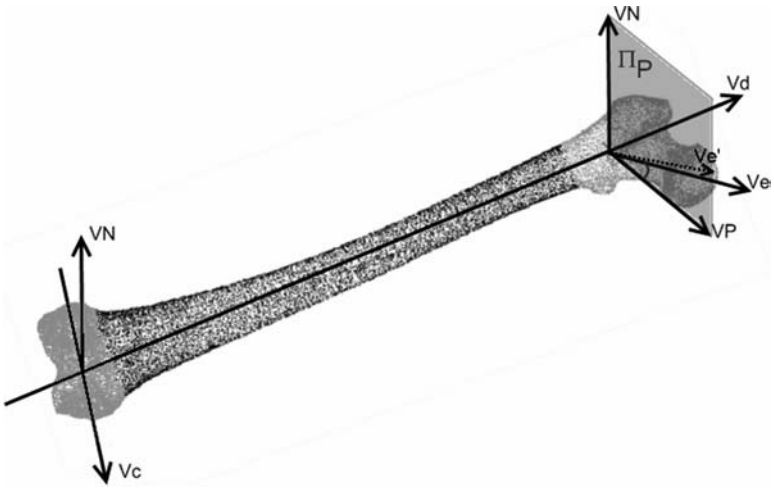

Figure 7. Cylinder centreline vectors of C, D and N regions, called $\boldsymbol{\nu}_C$, $\boldsymbol{\nu}_d$ and $\boldsymbol{\nu}_e$, respectively. $\boldsymbol{\nu}_N$ is the vector normal to $\boldsymbol{\nu}_C$ and $\boldsymbol{\nu}_d$. $\boldsymbol{\nu}_P$ is the vector normal to $\boldsymbol{\nu}_d$ and $\boldsymbol{\nu}_N$. Π_P is the projection plane formed by $\boldsymbol{\nu}_N$ and $\boldsymbol{\nu}_P$, in which anteversion angle is automatically measured.

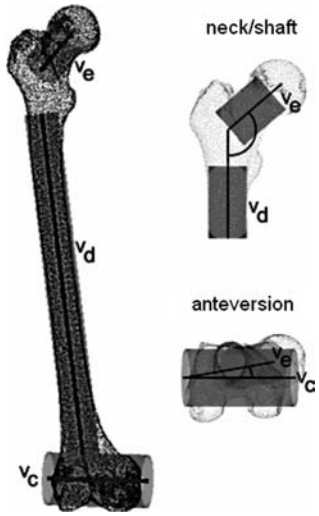

Figure 8. Cylinder fit to condylar, diaphyseal and epiphyseal regions and the corresponding axes defined by vectors $\boldsymbol{\nu}_C$, $\boldsymbol{\nu}_d$ and $\boldsymbol{\nu}_e$. $\boldsymbol{\nu}_d$ and $\boldsymbol{\nu}_e$ define the neck–shaft angle. Anteversion was defined between $\boldsymbol{\nu}_C$ and $\boldsymbol{\nu}_e$ projected into Π_P.

3. Results

We analysed 10 right and 10 left femurs. In two right femurs, the necks were injured and angles could not be measured. Femoral angles for the different methods are presented in Table I. Angles resulting from manual and automatic subdivision did not differ ($p = 0.72$ and $p = 0.58$ for anteversion and neck–shaft angles, respectively). In other words, the automatic subdivision matched the regions manually painted by an expert eye. In a paired *t*-test, anteversion values were equivalent between conventional and automatic method ($p = 0.45$). For conventional method, neck–shaft angle was significantly below automatic values ($p < 0.05$), with mean and maximum differences of $-1.9°$ and $-4.8°$, respectively. Automatic and conventional methods were positively correlated for anteversion ($r^2 = 0.87$, $p < 0.001$) and neck–shaft angle ($r^2 = 0.89$, $p < 0.001$). In residues plot, mean differences between methods were $-0.4 \pm 2.4°$ for anteversion and $-1.8 \pm 2.9°$ for neck–shaft angle with no linear tendencies (Figure 9). Finally, mean distances from

Table 1. Femoral angles measured using different methods.

Femoral angle	Methodology		
	Manual separation	Automatic separation	Conventional (Reikeras [15])
Anteversion	19.4 ± 5.9	19.8 ± 6.6	19.3 ± 6.4
Neck–shaft	129.6 ± 8.7	130.2 ± 8.6	128.3 ± 7.5*

Notes: $N = 18$. Values expressed as mean ± SD in degrees. *$p < 0.05$ paired t-test with respect to automatic.

femur surface points to adjusted cylinders were 5.5 ± 0.6, 3.5 ± 0.6 and 2.4 ± 0.4 mm for condyles, diaphysis and neck regions, respectively.

4. Discussion

In this study, we introduced a new fully automatic method to assess anteversion and neck–shaft angles in human femurs and tested it in dried bones. The procedure was completely user independent and did not require any manual intervention. Even the initial automatic orientation of the bones inside the scanner was done automatically. The computer software was easy to use and the whole process took an average time of 20 s per bone to calculate the two femoral angles using a standard PC. We found anteversion ≈20° and neck–shaft angle ≈130°. These results are in agreement with the literature values. Isaac et al. (1997) found neck–shaft angles of 127 ± 3° in 171 dried femurs. Toogood et al. (2009) assessed proximal femoral anatomy and found neck–shaft angles of 129 ± 6° ($n = 375$). In other reports, values for anteversion, measured with two different 3D methods, were 20 ± 9° ($n = 30$; Sugano et al. 1998) and 17 ± 11° ($n = 20$; Kim et al. 2000b). Our values for anteversion and neck–shaft angles are also within the range reported by Hoaglud et al. in Caucasian cadavers: −2° to 35° ($n = 112$) and neck–shaft angles 120–161° ($n = 52$), respectively (Hoaglund and Low 1980). Femoral angles depend on age and gender (Toogood et al. 2009). In that sense, our reported values seem realistic, taking into account the number of bones measured in our study and the age range (16–58 y.o.) of the subjects.

The proposed methodology includes an automatic region subdivision to separate the different parts of the femur. This is the main improvement with respect to our previous preliminary work, in which the cylinder fitting algorithm was introduced but the regions of the bone depended on a manual segmentation (Casciaro et al. 2010). We also modified the cylinder fitting method adapting it to the peculiarities of the different regions, i.e. the condylar

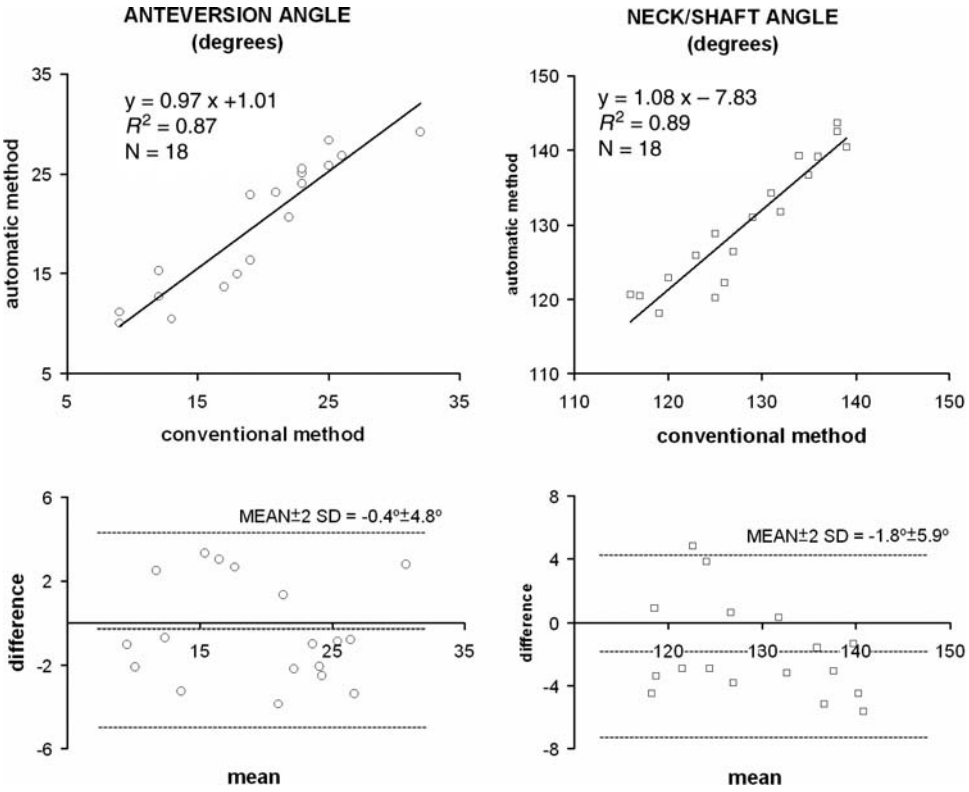

Figure 9. Correlation (top) and residues (bottom) plot for anteversion and neck–shaft angle using the conventional versus the automatic method.

region represents a closed surface. In addition, the automatic region subdivision could be used to estimate other femoral features than the angles. Length, volume or average diameter of each region can be easily calculated from the isolated 3D surface points and could be used to better describe the bone morphology in further protocols.

To validate the automatic subdivision, an independent expert, unaware of automatic measurements, manually segmented the neck, the diaphysis and the condyles. This manual procedure took about 20 min per bone. The resulting angles were equivalent between methods (Table I). In other words, the algorithm correctly matched the regions identified by the expert with no significant discrepancies in the angles assessment.

Conventional and automatic measurements were positively correlated. Anteversion was equivalent between methods although the neck–shaft angle in the automatic method was slightly above conventional method values. In all cases, the maximum discrepancies were below 5° with standard deviation of the mean below 3°. Evidently, the manual determination of the long neck, and condyles axes is subject to reader variability. Manually, the user must fix three axes, inside complex 3D structures, projected into virtual 2D planes. The resulting accuracy is difficult to predict. Comparisons between manual and automatic measures in other reports were in the range of 2–10° which emphasised the difficulty of assessing the neck axis accurately (Sugano et al. 1998; Kim et al. 2000b). The small differences between conventional and automatic measurements in our study were probably due to user variability in manual assessments. The key feature of our method is that it is 100% reproducible, offering a practical tool for clinical applications and avoiding user subjectivity.

Regarding the cylinder fitting method, we are aware that some of the structures do not strictly match with cylindrical shapes (Sugano et al. 1998; Schmutz et al. 2006; Toogood et al. 2009). We were inspired by Kim et al. (2000b) who used cylinders to fit the diaphysis and Sugano et al. (1998) who adjusted the femoral neck with a cylinder. In that sense, the cylindrical fit was a reasonable alternative. As expected, discrepancies between bone and cylinder surfaces were less important for neck and diaphysis with respect to condyles. Accordingly, average distances attained were 2.4 mm for the neck and 5.5 mm for condyles. It is to note that the definition of an angle requires two axes that are inscribed in a complicate anatomy. We believe that simplifying these regions with cylinders (and 'folding' and 'unfolding' some portions) was a valid choice that allowed us to straightforwardly identify these axes in a 3D hyperspace. From a cost–benefit perspective, cylinders were the simplest geometrical surfaces to fit the different portions of the femur. Even if bone morphology is complex, cylinders fix an individual axis that can be used to estimate femoral angles. Other 3D methods were numerically intensive or required some manual work (Sugano et al. 1998; Kim et al. 2000b). Conversely, fitting a cylinder to a group of surface points was less time consuming because it did not require any complex reconstructions.

At the moment, the region segmentation process and the angle assessment were only validated in dried human femurs. The automatic orientation of the bone is already contemplated in our algorithm, but further revisions should be proposed to extend this methodology *in vivo*. The main obstacle would be the separation of the femur from the knee, the hip and the surrounding soft tissue. Bone limits may be artefacted by soft tissues, joints and eventual implanted devices. In addition, deforming pathologies such as arthritis may introduce difficulties to analyse femoral angles *in vivo*. Most reports that carry out semi-automatic segmentation rely on thresholding (Kim et al. 2000a; Subburaj et al. 2009; Subburaj et al. 2010), although other automatic approaches can be found elsewhere (Jolly et al. 2010). These issues should be further explored in future studies although these adaptations may not introduce considerable modifications to the method core that seems potentially prepared for *in vivo* CT scans once the femur is isolated from the hip and the knee.

In conclusion, this study proposed a fully automatic method to estimate anteversion and neck–shaft angles from human femurs which was tested on dried bones. The automatic region segmentation and the angle assessment did not differ from manual separation and conventional angle estimation, respectively. The method was fast and did not require any user intervention, thus it is 100% reproducible. Further validations with a larger number of bones and adaptations for *in vivo* CT studies are expected in the near future to ensure a clinically compliant method.

Acknowledgement

The authors would like to thank Dr Lucas Ritacco for his invaluable assistance.

References

Birkenmaier C, Jorysz G, Jansson V, Heimkes B. 2010. Normal development of the hip: a geometrical analysis based on planimetric radiography. J Pediatr Orthop B. 19(1):1–8, Available from http://www.ncbi.nlm.nih.gov/entrez/query.fcgi?cmd=Retrieve&db=PubMed&dopt=Citation&list_uids=19829156. DOI 10.1097/BPB.0b013e32832f5aeb.

Casciaro ME, Ritacco LE, Milano F, Risk M, Craiem D. 2010. Angle estimation of human femora in a three-dimensional virtual environment. In: Proceedings of the Engineering in Medicine and Biology Society (EMBC), 2010 Annual International Conference of the IEEE; 2010 August 31 2010–September 4 2010; Buenos Aires, Argentina.

Citak M, Kendoff D, Pearle AD, O'Loughlin PF, Krettek C, Hufner T. 2009. Navigated femoral anteversion measure-

ments: general precision and registration options. Arch Orthop Trauma Surg. 129(5):671–677, Available from http://www.ncbi.nlm.nih.gov/entrez/query.fcgi?cmd=Retrieve&db=PubMed&dopt=Citation&list_uids=19132378. DOI 10.1007/s00402-008-0804-6.

Craiem D, Casciaro ME, Graf S, Glaser CE, Gurfinkel EP, Armentano RL. 2009. Coronary arteries simplified with 3D cylinders to assess true bifurcation angles in atherosclerotic patients. Cardiovasc Eng. 9(4):127–133, Available from http://www.ncbi.nlm.nih.gov/entrez/query.fcgi?cmd=Retrieve&db=PubMed&dopt=Citation&list_uids=19816773. DOI 10.1007/s10558-009-9084-1.

Gargouri I, de Guise JA. 2007. Automated method for clinic and morphologic analysis of bones using implicit modeling technique. In: Conf Proc IEEE Eng Med Biol Soc. 2007. p. 5095–5098, Available from http://www.ncbi.nlm.nih.gov/entrez/query.fcgi?cmd=Retrieve&db=PubMed&dopt=Citation&list_uids=18003152. DOI 10.1109/IEMBS.2007.4353486.

Gonzalez R, Woods RE. 1992. Digital image processing. Reading, MA: Addison-Wesley.

Hoaglund FT, Low WD. 1980. Anatomy of the femoral neck and head, with comparative data from Caucasians and Hong Kong Chinese. Clin Orthop Relat Res. (152):10–16, Available from http://www.ncbi.nlm.nih.gov/entrez/query.fcgi?cmd=Retrieve&db=PubMed&dopt=Citation&list_uids=7438592.

Hoiseth A, Reikeras O, Fonstelien E. 1989. Evaluation of three methods for measurement of femoral neck anteversion. Femoral neck anteversion, definition, measuring methods and errors. Acta Radiol. 30(1):69–73, Available from http://www.ncbi.nlm.nih.gov/entrez/query.fcgi?cmd=Retrieve&db=PubMed&dopt=Citation&list_uids=2914119.

Isaac B, Vettivel S, Prasad R, Jeyaseelan L, Chandi G. 1997. Prediction of the femoral neck-shaft angle from the length of the femoral neck. Clin Anat. 10(5):318–323, Available from http://www.ncbi.nlm.nih.gov/entrez/query.fcgi?cmd=Retrieve&db=PubMed&dopt=Citation&list_uids=9283729. DOI 10.1002/(SICI)1098-2353(1997)10:5<318:AID-CA5>3.0.CO;2-M [pii] 10.1002/(SICI)1098-2353(1997)10:5<318:AID-CA5>3.0.CO;2-M.

Jolly MP, Alvino C, Odry B, Deng X, Zheng J, Harder M, Guehring J. 2010. Automatic femur segmentation and condyle line detection in 3D MR scans for alignment of high resolution MR. In: Proceedings of the Biomedical Imaging: From Nano to Macro, 2010 IEEE International Symposium on 14–17 April 2010; Rotterdam, The Netherlands.

Kim JS, Park TS, Park SB, Kim IY, Kim SI. 2000a. Measurement of femoral neck anteversion in 3D. Part 1: 3D imaging method. Med Biol Eng Comput. 38(6):603–609, Available from http://www.ncbi.nlm.nih.gov/entrez/query.fcgi?cmd=Retrieve&db=PubMed&dopt=Citation&list_uids=11217876.

Kim JS, Park TS, Park SB, Kim IY, Kim SI. 2000b. Measurement of femoral neck anteversion in 3D. Part 2: 3D modelling method. Med Biol Eng Comput. 38(6):610–616, Available from http://www.ncbi.nlm.nih.gov/entrez/query.fcgi?cmd=Retrieve&db=PubMed&dopt=Citation&list_uids=11217877.

Lee DY, Lee CK, Cho TJ. 1992. A new method for measurement of femoral anteversion. A comparative study with other radiographic methods. Int Orthop.. 16(3):277–281, Available from http://www.ncbi.nlm.nih.gov/entrez/query.fcgi?cmd=Retrieve&db=PubMed&dopt=Citation&list_uids=1428343.

Pearle AD, Goleski P, Musahl V, Kendoff D. 2009. Reliability of image-free navigation to monitor lower-limb alignment. J Bone Joint Surg Am. 91(Suppl 1):90–94, Available from http://www.ncbi.nlm.nih.gov/entrez/query.fcgi?cmd=Retrieve&db=PubMed&dopt=Citation&list_uids=19182032. DOI 91/Supplement_1/90 [pii] 10.2106/JBJS.H.01439.

Schmutz B, Reynolds KJ, Slavotinek JP. 2006. Development and validation of a generic 3D model of the distal femur. Comput Methods Biomech Biomed Engin. 9(5):305–312, Available from http://www.ncbi.nlm.nih.gov/entrez/query.fcgi?cmd=Retrieve&db=PubMed&dopt=Citation&list_uids=17132616. DOI K75706Q0042W68M5 [pii] 10.1080/10255840600935217.

Subburaj K, Ravi B, Agarwal M. 2009. Automated identification of anatomical landmarks on 3D bone models reconstructed from CT scan images. Comput Med Imaging Graph. 33(5):359–368, Available from http://www.ncbi.nlm.nih.gov/entrez/query.fcgi?cmd=Retrieve&db=PubMed&dopt=Citation&list_uids=19345065. DOI S0895-6111(09)00024-X [pii] 10.1016/j.compmedimag.2009.03.001.

Subburaj K, Ravi B, Agarwal M. 2010. Computer-aided methods for assessing lower limb deformities in orthopaedic surgery planning. Comput Med Imaging Graph. 34(4):277–288, DOI 10.1016/j.compmedimag.2009.11.003.

Sugano N, Noble PC, Kamaric E. 1998. A comparison of alternative methods of measuring femoral anteversion. J Comput Assist Tomogr. 22(4):610–614, Available from http://www.ncbi.nlm.nih.gov/entrez/query.fcgi?cmd=Retrieve&db=PubMed&dopt=Citation&list_uids=9676454.

Tayton E. 2007. Femoral anteversion: a necessary angle or an evolutionary vestige? J Bone Joint Surg Br. 89(10):1283–1288, Available from http://www.ncbi.nlm.nih.gov/entrez/query.fcgi?cmd=Retrieve&db=PubMed&dopt=Citation&list_uids=17957064. DOI 89-B/10/1283 [pii] 10.1302/0301-620X.89B10.19435.

Toogood PA, Skalak A, Cooperman DR. 2009. Proximal femoral anatomy in the normal human population. Clin Orthop Relat Res. 467(4):876–885, Available from http://www.ncbi.nlm.nih.gov/entrez/query.fcgi?cmd=Retrieve&db=PubMed&dopt=Citation&list_uids=18758876. DOI 10.1007/s11999-008-0473-3.